

LETTERS

Silicon nanowires as efficient thermoelectric materials

Akram I. Boukai¹†, Yuri Bunimovich¹†, Jamil Tahir-Kheli¹, Jen-Kan Yu¹, William A. Goddard III¹ & James R. Heath¹

Thermoelectric materials interconvert thermal gradients and electric fields for power generation or for refrigeration^{1,2}. Thermoelectrics currently find only niche applications because of their limited efficiency, which is measured by the dimensionless parameter ZT —a function of the Seebeck coefficient or thermoelectric power, and of the electrical and thermal conductivities. Maximizing ZT is challenging because optimizing one physical parameter often adversely affects another³. Several groups have achieved significant improvements in ZT through multi-component nanostructured thermoelectrics^{4–6}, such as $\text{Bi}_2\text{Te}_3/\text{Sb}_2\text{Te}_3$ thin-film superlattices, or embedded PbSeTe quantum dot superlattices. Here we report efficient thermoelectric performance from the single-component system of silicon nanowires for cross-sectional areas of $10\text{ nm} \times 20\text{ nm}$ and $20\text{ nm} \times 20\text{ nm}$. By varying the nanowire size and impurity doping levels, ZT values representing an approximately 100-fold improvement over bulk Si are achieved over a broad temperature range, including $ZT \approx 1$ at 200 K. Independent measurements of the Seebeck coefficient, the electrical conductivity and the thermal conductivity, combined with theory, indicate that the improved efficiency originates from phonon effects. These results are expected to apply to other classes of semiconductor nanomaterials.

The most efficient thermoelectrics have historically been heavily doped semiconductors because the Pauli principle restricts the heat-carrying electrons to be close to the Fermi energy¹ for metals. The Wiedemann–Franz law, $\kappa_e/\sigma T = \pi^2/3(k/e)^2 = (156\text{ }\mu\text{V K}^{-1})^2$, where κ_e is the electronic contribution to κ , constrains $ZT = S^2\sigma T/\kappa$, where S is the Seebeck coefficient (or thermoelectric power, measured in VK^{-1}), and σ and κ are the electrical and thermal conductivities, respectively. Semiconductors have a lower density of carriers, leading to larger S values and a κ value that is dominated by phonons (κ_{ph}), implying that the electrical and thermal conductivities are somewhat decoupled¹. κ can be reduced by using bulk semiconductors of high atomic weight, which decreases the speed of sound. However, this strategy has not yet produced materials with $ZT > 1$.

For a metal or highly doped semiconductor, S is proportional to the energy derivative of the density of electronic states. In low-dimensional (nanostructured) systems the density of electronic states has sharp peaks^{7–9} and, theoretically, a high thermopower. Harnessing this electronic effect to produce high- ZT materials has had only limited success^{10,11}. However, optimization of the phonon dynamics and heat transport physics in nanostructured systems has yielded results^{4–6}. Nanostructures may be prepared with one or more dimensions smaller than the mean free path of the phonons and yet larger than that of electrons and holes. This potentially reduces κ without decreasing σ (ref. 12). Bulk silicon (Si) is a poor thermoelectric ($ZT_{300\text{ K}} \approx 0.01$; ref. 13), and this phonon physics is important for our Si nanowires, in which the electronic structure remains bulk-like.

Figure 1 shows images of the devices and the Si nanowires we used for these experiments. Details related to the fabrication, calibration and experimental measurements are presented in the Supplementary

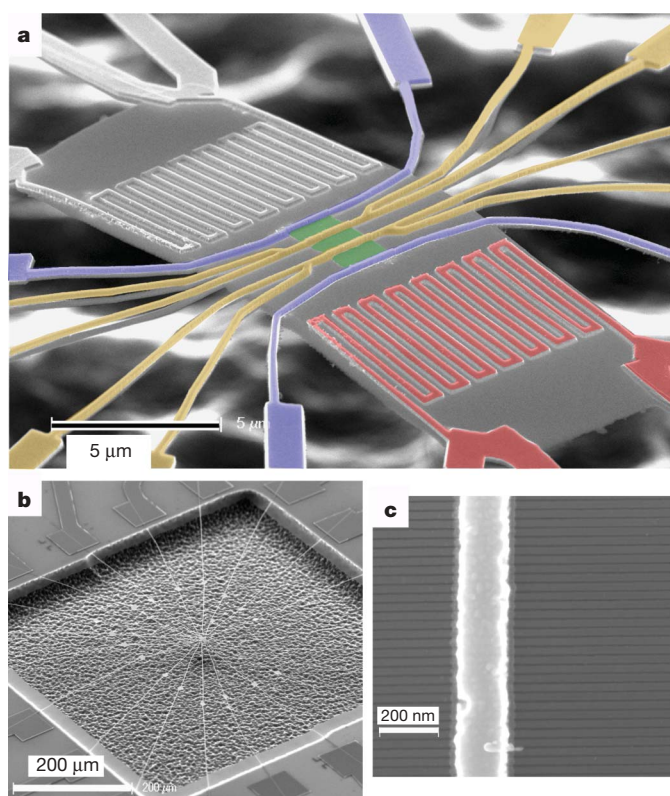


Figure 1 | Scanning electron micrographs of the device used to quantitate the thermopower and electrical and thermal conductivity of Si nanowire arrays. **a**, This false-colour image of a suspended platform shows all electrical connections. The central green area is the Si nanowire array, which is not resolved at this magnification. The four-lead yellow electrodes are used for thermometry to quantify the temperature difference across the nanowire array. The thermal gradient is established with either of the two Joule heaters (the right-hand heater is coloured red). The yellow and blue electrodes are combined to carry out four-point electrical conductivity measurements on the nanowires. The grey region underlying the nanowires and the electrodes is the 150-nm-thick SiO_2 insulator that is sandwiched between the top Si(100) single-crystal film from which the nanowires are fabricated, and the underlying Si wafer. The underlying Si wafer has been etched back to suspend the measurement platform, placing the background of this image out of focus. **b**, Low-resolution micrograph of the suspended platform. The electrical connections radiate outwards and support the device. **c**, High-resolution image of an array of 20-nm-wide Si nanowires with a Pt electrode.

¹Division of Chemistry and Chemical Engineering, MC 127-72, 1200 East California Blvd, California Institute of Technology, Pasadena, California 91125, USA.

†These authors contributed equally to this work.

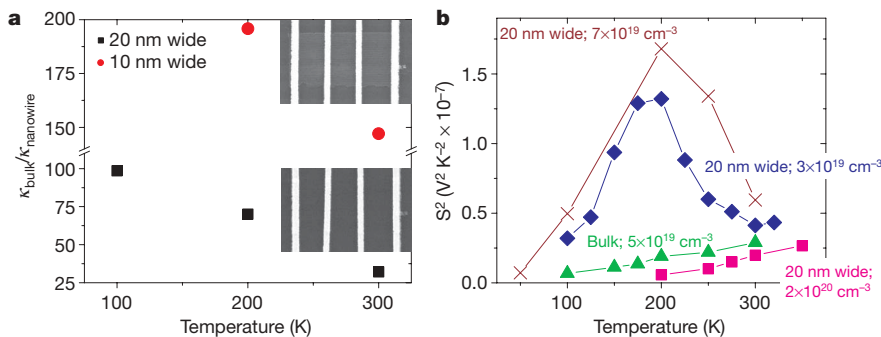


Figure 2 | Factors contributing to ZT for various Si nanowires. All nanowires are 20 nm in height. **a**, The temperature dependence of the thermal conductivity κ , presented as $\kappa_{\text{bulk}}/\kappa_{\text{nanowire}}$ to highlight the improvement that the reduction of κ in nanowires leads to ZT. κ_{bulk} values, which are slightly below the true bulk value for Si, are taken from an identically measured $520 \text{ nm} \times 35 \text{ nm}$ -sized film. The inset scanning electron microscope micrographs show the region of the device containing the nanowires before (top) and after (bottom) the XeF_2 etch to remove the

Information. The platform permits four-point measurements of the electrical conductivity of the nanowires, Joule heating to establish a thermal gradient across the nanowires, and four-point thermometry to quantify that gradient^{10,14}. The resistance of the four-point thermometry electrodes is typically two orders of magnitude smaller than the resistance of the nanowires. The measurement platform is suspended in vacuum to allow measurement of nanowire thermal conductivity^{15,16}. For all measurements, the Si nanowires could be selectively removed using a XeF_2 etch, thus allowing for measurements of the contributions to σ , S and κ from the platform and oxide substrate.

There are several ways to prepare Si nanowires, including materials methods for bulk production¹⁷. We wanted Si nanowires in which the dimensions, impurity doping levels, crystallographic nature, and so on, were all quantifiable and precisely controlled. We used the superlattice nanowire pattern transfer (SNAP) method¹⁸, which translates the atomic control over the layer thickness of a superlattice into control over the width and spacing of nanowires. Si nanowires made via SNAP inherit their impurity dopant concentrations directly from the single-crystal Si epilayers of the silicon-on-insulator substrates from which they are fabricated¹⁹. These epilayers were 20- or 35-nm-thick Si(100) films on 150 nm of SiO_2 , and were p-type impurity (boron) doped using diffusion-based doping¹⁹. Four-point probe conductivity measurements of the silicon-on-insulator films were used to extract dopant concentrations. We prepared nanowire arrays several micrometres long, with lateral width \times thickness dimensions of $10 \text{ nm} \times 20 \text{ nm}$, $20 \text{ nm} \times 20 \text{ nm}$ and $520 \text{ nm} \times 35 \text{ nm}$. The last approximates the bulk and, in fact, measurements on the sample obtained bulk values for S , σ and κ . Measurements of κ for our nanowires were consistent with literature values for materials grown (round) Si nanowires¹⁶.

All values of S , σ and κ reported here are normalized to individual nanowires, although each experiment used a known number of nanowires ranging from 10 to 400. The Si microwires and nanowires were prepared using the same substrates, doping methods, and so on, but different patterning methods (electron-beam lithography versus SNAP).

Measurements of κ and S^2 for Si nanowires (and microwires) for different nanowire sizes and doping levels are presented in Fig. 2. More complete data sets, electrical conductivity data and a statistical analysis are presented in the Supplementary Information. The nanowire electrical conductivity is between 10 and 90% of the bulk, depending on nanowire dimensions. A reduced σ probably arises from surface scattering of charge carriers¹⁹. Nevertheless, all nanowires are highly doped and most exhibit metallic-like conductivity (increasing σ with decreasing T).

nanowires. **b**, The temperature dependence of S^2 for 20-nm-wide Si nanowires at various p-type doping concentrations (indicated on the graph). Note that the most highly doped nanowires (pink line) yield a thermopower similar to that of bulk Si doped at a lower level. For nanowires doped at slightly higher and slightly lower concentrations than the bulk, S peaks near 200 K. This is a consequence of the one-dimensional nature of the Si nanowires.

The temperature dependence of κ for a microwire and 10- and 20-nm-wide nanowires were recorded at modest statistical resolution to establish trends. This data indicated that κ drops sharply with shrinking nanowire cross-section (Fig. 2a) and that the 10-nm-wide nanowires exhibited a κ value ($0.76 \pm 0.15 \text{ W m}^{-1} \text{ K}^{-1}$) that was below the theoretical limit of $0.99 \text{ W m}^{-1} \text{ K}^{-1}$ for bulk Si (ref. 20). Thus, very large data sets were collected for 10- and 20-nm-wide nanowires to allow for a more precise determination of κ .

Our observed high ZT for Si nanowires (Fig. 3) occurs because κ is sharply reduced and the phonon drag component of the thermopower S_{ph} becomes large. Below, we show that S_{ph} increases because of a three-dimensional to one-dimensional crossover of the phonons participating in phonon drag and decreasing κ . However, we first discuss why our measured κ at 300 K for 10-nm-wide Si nanowires is less than κ_{min} (ref. 20).

The derivation of κ_{min} assumes that the minimum path length of wavelength λ phonons is $\lambda/2$ and that the phonons are described by the Debye model using bulk sound speeds with no optical modes. The $\lambda/2$ value is an order-of-magnitude estimate and is difficult to determine precisely, much like the minimum electron mean free path used to calculate the Mott–Ioffe–Regel σ_{min} . Also, κ_{min} is proportional to the transverse and longitudinal acoustic speeds of sound²⁰. These are reduced in our nanowires at long wavelengths because the modes

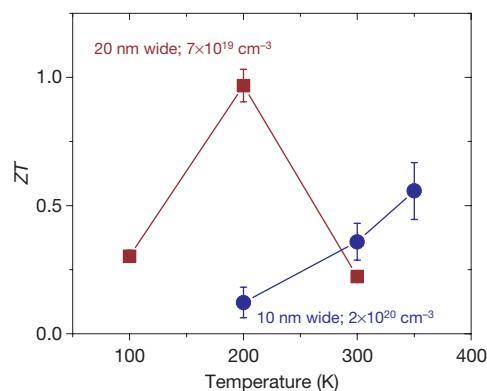


Figure 3 | Temperature dependence of ZT for two different groups of nanowires. The cross-sectional area of the nanowires, and the p-type doping level, are given. The 20-nm-wide nanowires have a thermopower that is dominated by phonon contributions, and a ZT value ~ 1 is achieved near 200 K. The smaller (10-nm-wide) nanowires have a thermopower that is dominated by electronic contributions. The ZT at 350 K is calculated using the thermal conductivity value for the 10-nm-wide nanowires at 300 K. The error bars represent 95% confidence limits.

become one-dimensional. The ratio of the one-dimensional to two-dimensional longitudinal speeds of sound is $[(1+\nu)(1-2\nu)/(1-\nu)]^{1/2} = 0.87$ where $\nu = 0.29$ is the Poisson ratio of Si. The transverse acoustic speed goes to zero at long wavelength because $\omega \propto k^2 d$ where d is the nanowire width²¹. Therefore, the bulk κ_{\min} estimate above is invalid for our nanowires and values smaller than κ_{\min} are attainable.

For all but the most highly doped nanowires, S peaks near 200 K (Fig. 2b). This peak is unexpected: similarly doped bulk Si exhibits a gradual decrease in S as T is reduced (green trace). For $T < 100$ K, a peaked $S(T)$ is observed for metals and lightly doped semiconductors and is due to phonon drag^{13,22,23}.

Phonon drag is generally assumed to vanish with decreasing sample dimensions because the phonon path length is limited by the sample size^{24–26}. This seems to eliminate phonon drag as the reason for the peak in our nanowires. We show below that the phonon wavelengths participating in drag are of the order of or larger than the wire width. This leads to a three-dimensional to one-dimensional crossover of these modes and removes the cross-sectional wire dimensions from limiting the phonon mean path (see Fig. 4 inset). The nanowire boundaries are incorporated into the one-dimensional mode and are not an obstacle to phonon propagation. Therefore, the limiting size becomes the wire length ($\sim 1 \mu\text{m}$) and phonon drag ‘reappears’ at very small dimensions.

In addition, classical elasticity theory²¹ is valid for the phonon wavelengths considered here²⁷, leading to thermoelastic damping^{21,28,29} of sound waves proportional to κ . Thus S_{ph} is further enhanced, owing to the observed reduced thermal conductivity κ . A detailed discussion is in the Supplementary Information.

It might seem that elasticity theory leads to a contradiction because κ is proportional to the mean phonon lifetime. If the phonon lifetimes increase as stated above, then κ should also increase. But

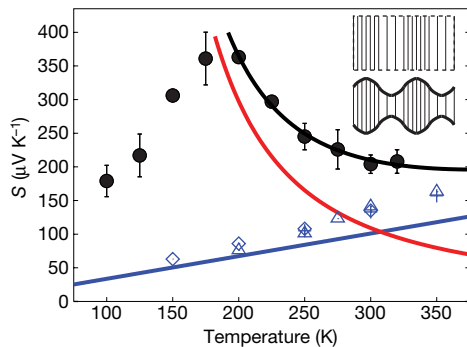


Figure 4 | Thermopower calculation plotted along with experimental data (black points) from a 20-nm-wide Si nanowire p-type doped at $3 \times 10^{19} \text{ cm}^{-3}$. The black curve is the fitted expression for the total thermopower $S_e + S_{\text{ph}}$. The red curve is the phonon contribution S_{ph} and the blue line is the electronic term S_e arising from the fit. The fit has maximum error $6.1 \mu\text{V K}^{-1}$ and root-mean-square error $1.8 \mu\text{V K}^{-1}$. The experimental error bars represent 95% confidence limits and at 150, 200 and 225 K are smaller than the data points. The blue data points are experimental values for bulk wires (doping $2 \times 10^{20} \text{ cm}^{-3}$; crosses), 10-nm-wide nanowires (doping $7 \times 10^{19} \text{ cm}^{-3}$; diamonds), and 20-nm-wide wires (doping $1.3 \times 10^{20} \text{ cm}^{-3}$; triangles) where only a linear- T electronic contribution was found. This data are close to the extracted electronic contribution from the black data points (blue line) and shows that the fitted linear term is reasonable. The drop in S to 0 as $T \rightarrow 0$ occurs because the phonon mean free path reaches the sample size and the specific heat tends to 0 according to the third law of thermodynamics. The inset shows the character of a three-dimensional bulk longitudinal acoustic phonon mode (top) and a one-dimensional mode when the wavelength is larger or of the order of the width (bottom). The one-dimensional mode incorporates the existence of the boundary by transverse expansion (or compression) for longitudinal compression (or expansion). The ratio of the transverse strain to the longitudinal strain is the Poisson ratio (0.29 for Si).

because the elasticity expression is only valid for long-wavelength modes, and κ is the average of all modes, there is no contradiction.

We now consider separately the electronic and phonon contributions to the thermopower— $S = S_e + S_{\text{ph}}$ —for the nanowire data at $T > 200$ K. Charge carriers dissipate heat to the lattice through a process that first involves momentum conserving (non-dissipative) electron–phonon collisions. The phonons that contribute to phonon drag cannot have a wavelength shorter than λ_{\min} , which is determined by the size of the Fermi surface. Phonon drag is observed in metals only at low T because the Fermi surface is large and the heat carrying short-wavelength phonons have short lifetimes. At low T (< 20 K), $S_{\text{ph}} \propto T^3$ from the phonon specific heat ($\propto T^3$). For $kT \gg \Theta_{\text{Debye}}$, the specific heat becomes constant and the number of phonons available for phonon–phonon scattering is $\propto T$, leading to $S_{\text{ph}} \propto 1/T$ (ref. 1).

For p-type Si, the holes are near the valence band maximum. The phonon drag modes are acoustic with the largest wavevector $k_{\text{ph}} = 2k_{\text{Fermi}} = 0.2 \text{ \AA}^{-1}$ (for impurity doping of $3 \times 10^{19} \text{ cm}^{-3}$). The shortest wavelength is $\lambda_{\text{ph}} = 2\pi/k = 31 \text{ \AA}$.

Umklapp (non-momentum-conserving) phonon–phonon scattering processes determine the rate of phonon heat dissipation. The Debye energy Θ_D sets the energy scale for Umklapp scattering. The number of Umklapp phonons available to dissipate the long-wavelength phonons is given by the Bose–Einstein function:

$$N_U = \frac{1}{e^{\Theta_D/T} - 1}$$

leading to a scattering rate $1/\tau_{\text{ph}} \propto N_U$. When $T \gg \Theta_D$, $1/\tau_{\text{ph}} \propto T$. Because $\Theta_D = 640$ K for Si, the full Bose–Einstein expression must be applied for $T \leq 350$ K. The electronic contribution S_e is estimated from the Mott formula¹:

$$S_e(T) = \frac{\pi^2 k^2 T}{3e} \left(\frac{\partial \ln \sigma(\epsilon)}{\partial \epsilon} \right) \approx (283 \mu\text{V K}^{-1}) (kT/E_F)$$

where the conductivity derivative equals the reciprocal of the energy scale over which it varies (the Fermi energy E_F). Assuming hole doping occurs in the heavier Si valence band (mass 0.49), this leads to $E_F = 0.072 \text{ eV} = 833 \text{ K}$ and $k_F = 0.1 \text{ \AA}^{-1}$ for the number density of boron dopant atoms $n = 3 \times 10^{19} \text{ cm}^{-3}$. Thus $S_e(T) = aT$ where $a = 0.34 \mu\text{V K}^{-2}$.

The $T > 200$ K thermopower data of the 20-nm-wide wire (doping $n = 3 \times 10^{19} \text{ cm}^{-3}$) fits:

$$S = S_e + S_{\text{ph}} = aT + b[\exp(\Theta_D/T) - 1]$$

where a , b and Θ_D are varied to obtain the best fit (Fig. 4). The coefficients are $a = 0.337 \mu\text{V K}^{-2}$, $b = 22.1 \mu\text{V K}^{-1}$, and $\Theta_D = 534$ K. The coefficient a is almost identical to our estimate of $0.34 \mu\text{V K}^{-2}$. Thus phonon drag explains the observed thermopower. Consistent with measurements²⁴ of phonon drag in bulk Si, S in our nanowires increases significantly at lighter doping. This data, plus a fit of the Fig. 4 data using the experimental $\Theta_D = 640$ K, is presented in the Supplementary Information. Rather than fitting by varying a , b and Θ_D , we fixed Θ_D to its known experimental value (640 K) and allowed only a and b to vary.

The phonon drag contribution to S is of the form^{23,30}:

$$S_{\text{ph}} \propto \left(\frac{\tau_{\text{ph}}}{\mu T} \right)$$

τ_{ph} , the phonon lifetime, is $\propto 1/\kappa$ from elasticity theory. μ is the electron mobility. ZT scales as (neglecting S_e):

$$S_{\text{ph}} \propto \frac{1}{\mu T \kappa}$$

$$\sigma \propto n \mu$$

$$ZT \propto \frac{n}{\mu T \kappa^3}$$

leading to increased ZT with decreasing mobility. This is the opposite conclusion reached from when we consider only S_e (ref. 7).

We have combined experiment and theory to demonstrate that semiconductor nanowires can be designed to achieve extremely large enhancements in thermoelectric efficiency, and we have shown that the temperature of maximum efficiency may be tuned by changing the doping and the nanowire size. Theory indicates that similar improvements should be achievable for other semiconductor nanowire systems because of phonon effects. These nanowire thermoelectrics may find applications related to on-chip heat recovery, cooling and power generation. Additional improvements through further optimization of nanowire size, doping and composition should be possible.

METHODS SUMMARY

Single-crystalline Si nanowires were fabricated using the SNAP process¹⁸. The nanowires were doped p-type using a boron-containing spin-on dopant (see Supplementary Information for details)¹⁹. Electron-beam lithography was used to create Ti/Pt electrodes for the electrical and heat transport measurements. The entire device was suspended using a XeF₂ etch, leaving the nanowires anchored to a thin SiO island (see Supplementary Information for details). The nanowire electrical conductivity was measured by a Keithley 2400 using a four-point measurement to eliminate contact resistance. For measurement of S and κ , a temperature difference was created across the ends of the nanowires by sourcing a direct current through one of the resistive heaters. The resistance rise of each thermometer was recorded simultaneously using a lock-in measurement (Stanford Research Systems SRS-830) as the temperature was ramped upwards. The resistance of the thermometers was typically two orders of magnitude smaller than the nanowire array. For measurement of S , the thermoelectric voltage, as a response to the temperature difference, was recorded using a Keithley 2182A nanovoltmeter. A difference measurement was used to determine κ , whereby the κ value of the nanowires plus the oxide island was subtracted from the κ value of the oxide island. The thermal conductivity of the oxide island was determined by removing the nanowires with a highly selective XeF₂ etch (see Supplementary Information for details).

Received 15 June; accepted 2 November 2007.

- MacDonald, D. K. C. *Thermoelectricity: An Introduction to the Principles* (Wiley, New York, 1962).
- Mahan, G., Sales, B. & Sharp, J. Thermoelectric materials: New approaches to an old problem. *Phys. Today* **50**, 42–47 (1997).
- Chen, G. *et al.* Recent developments in thermoelectric materials. *Int. Mater. Rev.* **48**, 45–66 (2003).
- Venkatasubramanian, R. *et al.* Thin-film thermoelectric devices with high room-temperature figures of merit. *Nature* **413**, 597–602 (2001).
- Harman, T. C. *et al.* Quantum dot superlattice thermoelectric materials and devices. *Science* **297**, 2229–2232 (2002).
- Hsu, K. F. *et al.* Cubic AgPb_mSbTe_{2+m}: Bulk thermoelectric materials with high figure of merit. *Science* **303**, 818–821 (2004).
- Hicks, L. D. & Dresselhaus, M. S. Thermoelectric figure of merit of a one-dimensional conductor. *Phys. Rev. B* **47**, 16631–16634 (1993).
- Mahan, G. D. & Sofo, J. O. The best thermoelectric. *Proc. Natl Acad. Sci. USA* **93**, 7436–7439 (1996).
- Humphrey, T. E. & Linke, H. Reversible thermoelectric nanomaterials. *Phys. Rev. Lett.* **94**, 096601 (2005).

- Boukai, A., Xu, K. & Heath, J. R. Size-dependent transport and thermoelectric properties of individual polycrystalline bismuth nanowires. *Adv. Mater.* **18**, 864–869 (2006).
- Yu-Ming, L. *et al.* Semimetal-semiconductor transition in Bi_{1-x}Sb_x alloy nanowires and their thermoelectric properties. *Appl. Phys. Lett.* **81**, 2403–2405 (2002).
- Majumdar, A. Enhanced thermoelectricity in semiconductor nanostructures. *Science* **303**, 777–778 (2004).
- Weber, L. & Gmelin, E. Transport properties of silicon. *Appl. Phys. A* **53**, 136–140 (1991).
- Small, J. P., Perez, K. M. & Kim, P. Modulation of thermoelectric power of individual carbon nanotubes. *Phys. Rev. Lett.* **91**, 256801 (2003).
- Li, S. *et al.* Measuring thermal and thermoelectric properties of one-dimensional nanostructures using a microfabricated device. *J. Heat Transf.* **125**, 881–888 (2003).
- Li, D. *et al.* Thermal conductivity of individual silicon nanowires. *Appl. Phys. Lett.* **83**, 2934–2936 (2003).
- Morales, A. M. & Lieber, C. M. A laser ablation method for the synthesis of semiconductor crystalline nanowires. *Science* **279**, 208–211 (1998).
- Melosh, N. A. *et al.* Ultra-high density nanowire lattices and circuits. *Science* **300**, 112–115 (2003).
- Wang, D., Sheriff, B. A. & Heath, J. R. Complementary symmetry silicon nanowire logic: Power-efficient inverters with gain. *Small* **2**, 1153–1158 (2006).
- Cahill, D. G., Watson, S. K. & Pohl, R. O. Lower limit to the thermal conductivity of disordered crystals. *Phys. Rev. B* **46**, 6131–6140 (1992).
- Landau, L. D. & Lifshitz, E. M. in *Theory of Elasticity* 3rd edn, 138 (Butterworth Heinemann, Oxford, 1986).
- Pearson, W. B. Survey of thermoelectric studies of the Group 1 metals at low temperatures carried out at the National Research Laboratories, Ottawa. *Sov. Phys. Solid State* **3**, 1024–1033 (1961).
- Herring, C. Theory of the thermoelectric power of semiconductors. *Phys. Rev.* **96**, 1163–1187 (1954).
- Geballe, T. H. & Hull, G. W. Seebeck effect in silicon. *Phys. Rev.* **98**, 940–947 (1955).
- Behnen, E. Quantitative examination of the thermoelectric power of n-type Si in the phonon drag regime. *J. Appl. Phys.* **67**, 287–292 (1990).
- Trzcinski, R., Gmelin, E. & Queisser, H. J. Quenched phonon drag in silicon microcontacts. *Phys. Rev. Lett.* **56**, 1086–1089 (1986).
- Maranganti, R. & Sharma, P. Length scales at which classical elasticity breaks down for various materials. *Phys. Rev. Lett.* **98**, 195504 (2007).
- Lifshitz, R. & Roukes, M. L. Thermoelastic damping in micro- and nanomechanical systems. *Phys. Rev. B* **61**, 5600–5609 (2000).
- Zener, C. Internal friction in solids. I. Theory of internal friction in reeds. *Phys. Rev.* **52**, 230–235 (1937).
- Gurevich, L. The thermoelectric properties of conductors. *Zhurnal Eksperimentalnoi i Teoreticheskoi Fiziki* **16**, 193–228 (1946).

Supplementary Information is linked to the online version of the paper at www.nature.com/nature.

Acknowledgements We thank D. Wang for discussions and J. Dionne, M. Roy, K. Kan and T. Lee for fabrication assistance. This work was supported by the Office of Naval Research, the Department of Energy, the National Science Foundation, the Defense Advanced Research Projects Agency, and a subcontract from the MITRE Corporation.

Author Contributions A.I.B., Y.B., J.-K.Y. and J.R.H. contributed primarily to the design and execution of the experiments. J.T.-K. and W.A.G. contributed primarily to the theory.

Author Information Reprints and permissions information is available at www.nature.com/reprints. Correspondence and requests for materials should be addressed to J.R.H. (heath@caltech.edu).